Metamagnetism and nanosize effects in the magnetic properties of the quasi-two-dimensional system β-Ni(OH)$_2$

James D. Rall and M. S. Seehra*
Department of Physics, West Virginia University, Morgantown, West Virginia 26506-6315, USA

E. S. Choi
Department of Physics and National High Magnetic Field Laboratory, Florida State University, Tallahassee, Florida 32310-3706, USA

(Received 18 May 2010; revised manuscript received 19 August 2010; published 2 November 2010)

Details of structural and magnetic properties of a sample of β-Ni(OH)$_2$ with nanoplate morphology (sample A) are compared with those of the hydrothermally synthesized bulklike β-Ni(OH)$_2$, sample B. Transmission electron microscopy, x-ray diffraction, infrared spectroscopy, and thermogravimetric analysis were used for structural characterization whereas studies of magnetic properties covered the temperature range of 2–350 K in magnetic fields upto H=180 kOe. Temperature dependence of the low-field susceptibilities, χ(ZFC) and χ(FC), showed that χ(ZFC) peak at T_P=24.5 K (26.5 K) for sample A (B) with χ(FC)$>\chi$(ZFC) below T_p. Curie-Weiss fit of χ(ZFC) for $T>T_P$ for sample A (B) yields θ=20.5 K (19.8 K) and magnetic moment μ =2.92 μ_B (3.30 μ_B)/Ni^{2+}. Measurements of the magnetization M vs H for $T<T_P$ for sample A show a two-step transition to ferromagnetism with the first transition at $H_{C1}\simeq$28 kOe and the second transition at $H_{C2}\simeq$55 kOe. For sample B, the transition at H_{C1} is absent and H_{C2}=53.5 kOe. Using molecular-field approach and three exchange constants determined from the Curie-Weiss fits, theoretical expressions for H_{C1} and H_{C2} are derived from which estimates of H_{C1} and H_{C2} are found to be in good agreement with the experimental values. According to this model, bulk β-Ni(OH)$_2$ orders antiferromagnetically (AF) at T_N $\simeq$25.5 K, with the dominant intralayer ferromagnetic (FM) coupling and a weaker interlayer AF coupling resulting in metamagnetism and FM ordering for $H\geq H_{C2}$. Nanosize effects are shown to lower T_P and T_N while also producing the transition at H_{C1} due to flipping of the surface layer Ni^{2+} spins.

DOI: 10.1103/PhysRevB.82.184403 PACS number(s): 75.30.Kz, 75.50.Tt, 75.50.Ee

I. INTRODUCTION

Magnetic properties of materials in lower than three dimensions (3D) such as layers and thin films [two-dimensional (2D)],[1] wires (one-dimensional),[2] and nanoparticles (zero-dimensional)[3,4] differ substantially from materials crystallizing in 3D because of the effects of dimensionality and the increasing role of surface atoms whose fraction increases as the dimension is reduced. Consequently, properties of such materials have attracted enormous attention in recent years with nanoparticles (NPs) being the focus of special interest because of their interesting properties and potential applications in areas such as information storage, catalysis, sensors, magnetic refrigeration, ferrofluids, and biomedicine.[3–5]

The two hydroxides of Ni, viz., α-Ni(OH)$_2$ and β-Ni(OH)$_2$ crystallize in the layered hexagonal CdI$_2$ structure [Fig. 1(a)] with the c axis being larger in the α phase because of the incorporation of additional (OH)$^-$ groups and other dopants during synthesis.[6,7] Even in the more stable β-Ni(OH)$_2$ with $a\simeq$3.12 Å and $c\simeq$4.60 Å, faults in the stacking of the (OH)$^-$ groups between the Ni^{2+} layers in the (00ℓ) planes are not uncommon.[7] Interestingly, these stacking faults result in the potential use of these hydroxides as positive electrode materials in nickel-based alkaline batteries.[7,8]

Regarding the magnetic properties of β-Ni(OH)$_2$, magnetic and neutron-diffraction studies have reported it to order antiferromagnetically (AFM) at T_N=25.75 K with the Ni^{2+} moments in the (00ℓ) planes ordered ferromagnetically (FM) along the c axis with the neighboring (00ℓ) planes ordered antiferromagnetically.[6,9,10] Magnetic studies by Takada *et al.*[10] showed a transition to metamagnetism at H_C=55 kOe (5.5 T) at 4.2 K.[10] In a recent work on 8.2 (2.1) nm NPs of β-Ni(OH)$_2$ with admittedly arbitrary shapes and sizes, Ti-

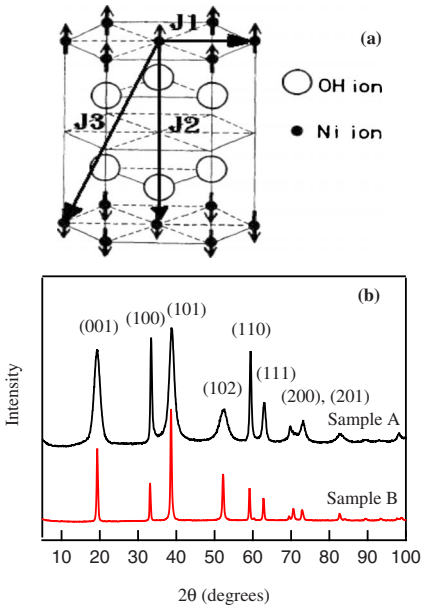

FIG. 1. (Color online) (a) Crystal structure of β-Ni(OH)$_2$ with the CdI$_2$ structure (adapted from Ref. 10). (b) Room-temperature XRD patterns for the powder samples with the Miller indices shown for the CdI$_2$ structure.

wari and Rajeev[11] concluded a paramagnetic to ferromagnetic transition near 26 K in their sample without referring to the above-mentioned earlier studies.[6,9,10] These conflicting reports about the nature of magnetism in β-$Ni(OH)_2$ motivated us to carry out more thorough investigations.

In this paper, we present the results of our detailed investigations on the nature of magnetism in β-$Ni(OH)_2$ by investigating two samples: a commercial powder sample from Alfa Aesar (sample A) with nanoplate morphology and a hydrothermally laboratory-synthesized bulk sample (sample B). Prior to magnetic studies, detailed structural characterizations of the samples were carried out using x-ray diffraction (XRD), transmission electron microscopy (TEM), thermogravimetric analysis (TGA), and infrared (IR) spectroscopy. These investigations showed sample A to be nanoplates of about 30 (10) nm size with thickness of about 3 (1) nm. Also, the samples are pure β-$Ni(OH)_2$ without any measurable contamination from nitrates or carbonates. Furthermore, larger β-$Ni(OH)_2$ particles, sample B, were synthesized hydrothermally to compare with sample A for particle size effects. Detailed investigations of the magnetic behavior in sample A from 2 to 350 K and in magnetic fields up to 180 kOe shows that in this sample transition to AFM order with change in temperature occurs in two steps: FM 2D ordering of the (00ℓ) sheets at $T_1 \simeq 25$ K followed by a 3D AFM order at the slightly lower temperature of $T_2 \simeq 23$ K. Variation in the magnetization (M) of sample A with applied magnetic field (H) shows a two-step transition from AFM to FM order at $H_{C1} \simeq 28$ kOe and $H_{C2} \simeq 55$ kOe. Using molecular-field approach and evaluated exchange constants, theoretical interpretation and estimates of H_{C1} and H_{C2} are found to be in good agreement with the experimental values. For sample A, the hysteresis loops for the zero-field-cooled (ZFC) and field-cooled (FC) cases are measured and temperature dependence of coercivity (H_c) and remanence (M_r) along with temperature dependence of H_{C1} and H_{C2} between 2 K and T_N are reported. Variation in M vs H up to 180 kOe shows saturation above 150 kOe in sample A with saturation magnetization $M_s = 118$ emu/g in good agreement with theoretical estimate for complete FM order. For bulklike sample B, the remanence and coercivity are negligible, and the magnetic field-induced transition at H_{C1} is absent with $H_{C2} = 53.5$ kOe. Overall, β-$Ni(OH)_2$ is found to be a metamagnet which can display some features of FM order resulting from the dominant in-plane exchange interaction in samples of nanometer dimensions. In the following pages, details of these results are presented, discussed, and interpreted in the context of previous studies mentioned earlier.[6,9–11]

II. SYNTHESIS AND STRUCTURAL CHARACTERIZATION OF β-$Ni(OH)_2$

Sample A, a commercial powder sample of β-$Ni(OH)_2$ from Alfa Aesar, was used without any further modifications, while sample B was grown hydrothermally from a precipitated solution. To prepare sample B, 4M NaOH was added dropwise to a magnetically stirred 125 ml aqueous solution of 0.1M $Ni(NO_3)_2 \cdot 6H_2O$ at room temperature until the liquid's pH=14. The precipitated $Ni(OH)_2$ and the solution was then transferred to a stainless steel 300 ml capacity autoclave and held at a temperature of 310 °C for 4 h after an initial ramp from room temperature of 1 h. The autoclave was cooled to room temperature naturally for 2 h. The precipitate was centrifuged, twice washed with deionized water and ethanol, and then dried at room temperature overnight.

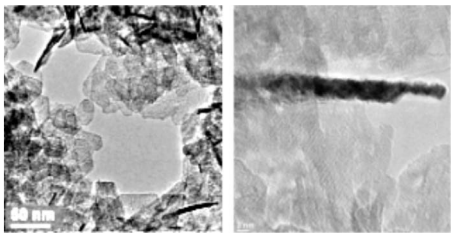

FIG. 2. Micrographs of TEM images of the powder β-$Ni(OH)_2$ sample A (adapted from Ref. 12). The estimated diameter of the plates is determined from (a) while the nanoplate thickness is determined from (b). The overall size of the images is also listed.

Visual views of sample A in the TEM micrographs of Fig. 2 show its nanoplate morphology with the plate sizes varying between about 20–40 nm and the plate thickness of about 3 (1) nm. The selective broadening of the different Bragg lines in the XRD pattern expected from thin-plate morphology is evident in the XRD pattern of Fig. 1(b). After correction for the instrumental broadening, the full width at half maximum linewidth (β_1) of the (001) Bragg line for sample A can be used to determine the approximate plate thickness from the Scherrer law: $d = \frac{0.9\lambda}{\beta_1 \cos\theta_1}$ (Ref. 13) yielding $d = 4.3$ nm with $\lambda = 0.154185$ nm being the wavelength of the Cu $K\alpha$ radiation used in the experiments (Rigaku diffractometer). Similarly, the plate size L is determined from the width (β_2) of the (100) line using $L = \frac{1.84\lambda}{\beta_2 \cos\theta_2}$ yielding $L = 33$ nm.[13] The magnitudes of L and d are consistent with the magnitudes estimated from TEM in Fig. 2. The widths of the mixed indices lines such as (101) and (102) in Fig. 1(b) can be explained similarly. The reader should take notice of the similar nonuniform broadening of the Bragg lines of the 8 nm β-$Ni(OH)_2$ sample in Ref. 11. In the earlier studies of β-$Ni(OH)_2$, the TEM data presented a similar morphology of their samples to ours (hexagonal plateletlike).[10] The lattice parameters of $a = 0.312$ nm and $c = 0.467$ nm were determined from the XRD pattern shown in Fig. 1(b) for sample A. For sample B, the XRD pattern [Fig. 1(b)] shows narrow lines characteristic of a bulklike sample. Using Scherrer law and the instrument correct linewidth, analysis similar to that used for sample A yields $L \simeq 72$ nm and thickness $d \simeq 24$ nm. These are likely the lower limits for sample B because of the comparable magnitudes of sample linewidths and instrumental broadening.

With the use of TGA, in which a sample's weight is measured while being heated in air at a constant rate, Ramesh *et al.*[7] inferred that their samples investigated for the electrochemical activity had the general formula $Ni(OH)_2 \cdot nH_2O$ which transformed to NiO near 300 °C,[14] where $n = 0.16–0.45$ was found for different samples. Similar TGA measurements were carried out on our samples, where the

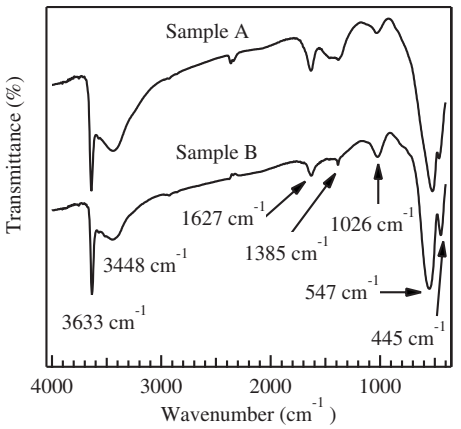

FIG. 3. IR spectroscopy of both samples. See text for the identification of the IR bands.

data were taken using a Mettler TG30 system at the heating rate of 5 °C/min for both samples. The expected weight loss for the $Ni(OH)_2 \rightarrow NiO$ transition is 19.4% in close agreement with the obtained data (not shown here) for both samples. The XRD pattern of the residual sample obtained after heating sample A to 500 °C shows it to be pure NiO. We also measured the IR spectra of both samples using both the KBr (potassium bromide) pellet method and photoacoustic spectroscopy employing a Mattson Infinity spectrometer. The observed transmittance bands shown in Fig. 3 are assigned as follows:[15,16] the sharp 3633 cm^{-1} band to free $\nu_{O\text{-}H}$ stretching in the OH group [see Fig. 1(a)]; the broad band centered around 3448 cm^{-1} to absorbed water; the 1627 cm^{-1} band to δ_{H_2O} bending from absorbed H_2O; the 1385 cm^{-1} band to Ni-O stretching; the 547 cm^{-1} band to $\delta_{O\text{-}H}$ bending in the OH group; and the 445 cm^{-1} band to Ni-O bending. The source of the 1026 cm^{-1} band in both samples is not yet certain. Exactly the same bands were observed using photoacoustic spectroscopy in which the powder sample is used as is, without any KBr. After determining the amount of surface absorbed water from TGA, our samples have the formula of β-$Ni(OH)_2 \cdot nH_2O$ with $n=0.15$ for sample A and $n=0.07$ for sample B.

III. EXPERIMENTAL RESULTS ON MAGNETIC PROPERTIES

Measurements of the magnetization (M) of sample A and sample B as a function of temperature and applied magnetic field (H) are presented next. Measurements up to 65 kOe were done using an in-house commercial superconducting quantum interference device (SQUID) magnetometer. Measurements up to 180 kOe on sample A were carried out at the National High Magnetic Field Laboratory (NHMFL) in Tallahassee, FL. In the measurements reported for the ZFC case, the sample is cooled in the absence of a field to 2 K, a measuring magnetic field (H) is then applied followed by acquisition of the M vs T data after stabilizing the temperature at each T. After reaching 350 K, the data of M vs T is then taken similarly with decreasing T in the same applied magnetic field (H), this being labeled as the FC case. All the

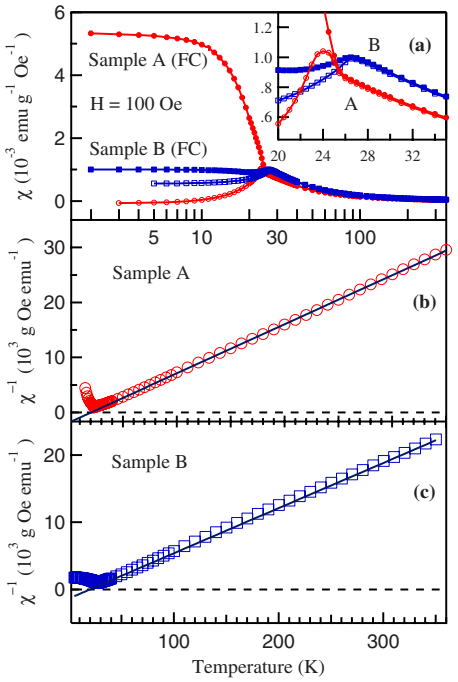

FIG. 4. (Color online) Temperature variations in (a) magnetic susceptibility ($\chi=M/H$, $H=100$ Oe) on a linear-log scale; (b) $1/\chi$ vs T data for the ZFC case with the solid line for the Curie-Weiss fit for sample A; (c) $1/\chi$ vs T data for the ZFC case with the solid line for the Curie-Weiss fit for sample B.

data presented here are corrected for the small magnetic field-independent diamagnetic susceptibility ($=-2.3 \times 10^{-8}$ emu/Oe) of the sample holder.

A. Temperature dependence

Variation in the magnetic susceptibility $\chi(=\frac{M}{H})$ as a function of temperature for the ZFC and FC cases with applied magnetic field $H=100$ Oe for sample A (sample B) in Fig. 4 shows that χ(ZFC) peaks at $T_p \simeq 24.5$ K (26.5 K) and that $\chi(FC) > \chi(ZFC)$ below T_p. For sample A, bifurcation of χ(ZFC) and χ(FC) occurs at slightly higher temperature than T_p; however for sample B, χ(FC) separates from χ(ZFC) at the peak temperature [inset of Fig. 4(a)]. In fact, χ(FC) has a peak at the same temperature as χ(ZFC). In the earlier studies[6,10] on bulklike β-$Ni(OH)_2$, $T_p \simeq 27$ K was reported, whereas in the recent studies on the average 8 nm NPs, $T_p \simeq 18$ K was found.[11] So our sample B is bulklike in its magnetic properties, whereas in sample A, there is a slight reduction of T_p because of its nanosize. Such a decrease in the ordering temperature with decrease in crystallite size has been observed in a number of systems[17] and interpreted in terms of finite size effects.[18] Additional discussion on the nanosize effects in β-$Ni(OH)_2$ is given later in Sec. IV.

To determine the nature of the transition at T_p, we measured the temperature dependence of the ac susceptibilities χ' and χ'' at frequencies $f=0.1$, 100, and 500 Hz looking for measurable changes in T_p with change in f for sample A. A systematic increase in T_p with increase in f is characteristic of noninteracting nanoparticles if T_p represent a blocking

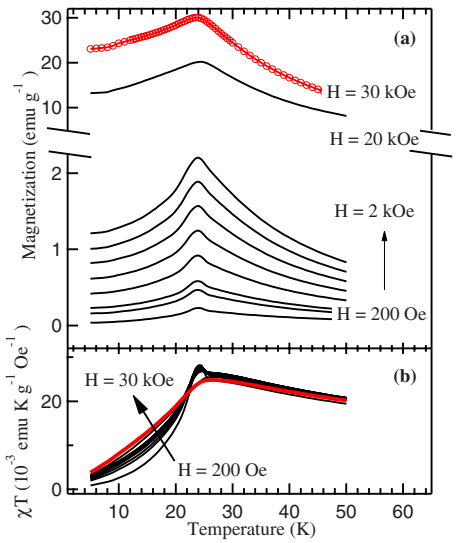

FIG. 5. (Color online) Temperature variation in the (a) magnetization and (b) χT for sample A. The curves are taken for applied magnetic fields of H=0.2, 0.4, 0.5, 0.8, 1.1, 1.4, 1.7, 2.0, 20, and 30 kOe. Typical data is shown for the 30 kOe case.

temperature.[19] However, for our sample A, T_p was found to be independent of f within experimental uncertainty of ± 0.25 K. This suggests that in the present case, T_p represents onset of bulk magnetic ordering due to strong interparticle interaction.[19]

For $T > T_p$, the χ(ZFC)=χ(FC) data are fitted to the Curie-Weiss law, $\chi = \frac{C}{(T-\theta)}$, with the plot of χ^{-1} vs T shown in Fig. 4(b) for sample A. The observed linear fit yields θ =20.5 K and $C = 112 \times 10^{-4}$ emu K/(g Oe). Using $C = N\mu^2/(3\ k)$, with $\mu^2 = g^2\mu_B^2 S(S+1)$ and g=2.2 for Ni^{2+}(μ_B is the Bohr magnetron) yields S=0.92 for β-$Ni(OH)_2 \cdot 0.15H_2O$. The slight departure from the expected S=1 magnitude for Ni^{2+} ions is likely due to the zero-point spin deviation which has also been observed in NiO system.[20] The magnitude of μ=2.92 μ_B/Ni^{2+} observed here nearly equals μ=2.98 μ_B/Ni^{2+} ion reported in Ref. 11 for the 8 nm NPs and μ=3.1 μ_B/Ni^{2+} ion reported in Ref. 6. Similar Curie-Weiss fit for sample B in Fig. 4(c) yields θ =20 K and μ=3.33 μ_B/Ni^{2+} ion. The positive θ reported here and in previous studies signifies that the dominant exchange interaction between Ni^{2+} ions in β-$Ni(OH)_2$ is ferromagnetic, even though the overall ordering is antiferromagnetic as shown by the neutron diffraction investigations[9] and discussed later.

Since results for bulklike sample B are identical to those reported in previous studies,[6,10] we focused primarily on sample A with nanoplate morphology. For sample A, M vs T data for the ZFC case in ten different magnetic fields (H) between H=50 Oe and H=30 kOe are shown in Fig. 5(a). The peak position T_p does not appear to shift much with variation in H. It is known that in AFMs, the Neel temperature T_N does not coincide with T_p; it is instead given by the peak in $\frac{\partial(\chi T)}{\partial T}$.[21] Plots of χT vs T for different magnetic fields obtained from the data in Fig. 5(a) are shown in Fig. 5(b). The computed magnitudes of $\frac{\partial(\chi T)}{\partial T}$ vs T for different H [Fig. 6(b)] shows a negative minimum and a positive maximum.

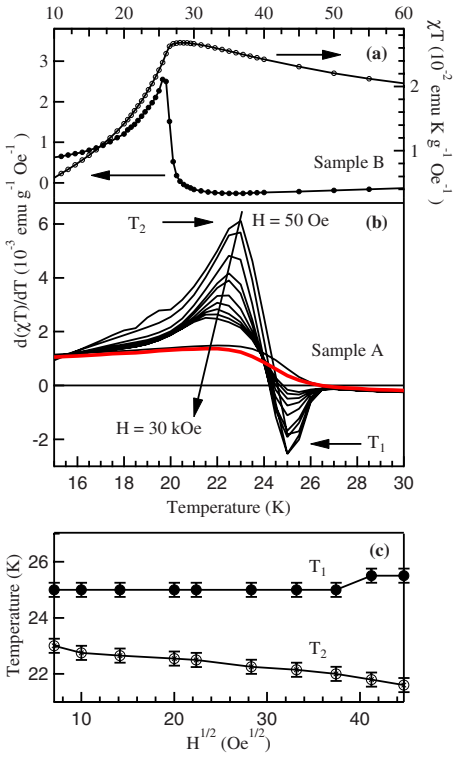

FIG. 6. (Color online) (a) Plot of χT vs T and computed $d(\chi T)/dT$ for sample B for the χ(ZFC) data at H=100 Oe. (b) Temperature variation in $d(\chi T)/dT$ for sample A with the arrow showing the approximate position of T_2 for H=0.05, 0.1, 0.2, 0.4, 0.5, 0.8, 1.1, 1.4, 1.7, 2.0, 20, and 30 kOe; (c) the corresponding applied magnetic field variation in the 2D FM transition (T_1) and the 3D AFM transition (T_2).

This observation is not typical of AFMs where only a positive maximum is reported at $T=T_N$.[22] We suggest that behavior of this sample is not typical of an AFM since for $T > T_N$, $\chi = \frac{C}{(T-\theta)}$ is observed with a positive θ as a result of the dominant FM interaction as shown earlier. A straightforward calculation from this Curie-Weiss variation yields

$$\frac{\partial(\chi T)}{\partial T} = -\frac{C\theta}{(T-\theta)^2}. \quad (1)$$

For positive θ, Eq. (1) yields a negative minimum at T=θ, and for negative θ typical of most AFMs with dominant AFM exchange interaction, $\frac{\partial(\chi T)}{\partial T}$ gives a positive maximum as observed experimentally in a number of AFMs.[22] Following this reasoning, we suggest that T_1 in Fig. 6(b) represents 2D ferromagnetic ordering of the Ni^{2+} moments in the (00ℓ) sheets, whereas long-range 3D AFM order occurs at the lower temperature (T_2). Variations in T_1 and T_2 against H for sample A are shown in Fig. 6(c). Such a two-step ordering observed here for β-$Ni(OH)_2$ is typical of layered AFMs (Ref. 1) although the dominant FM coupling in β-$Ni(OH)_2$ makes this system relatively unique. In the specific heat studies of bulklike β-$Ni(OH)_2$ in Ref. 6, this 2D to 3D ordering was also evident on approach to T_N from logarithmic divergence at higher T to 3D Ising-type behavior close to T_N. For bulklike sample B, plots of χT vs T using χ(ZFC) and com-

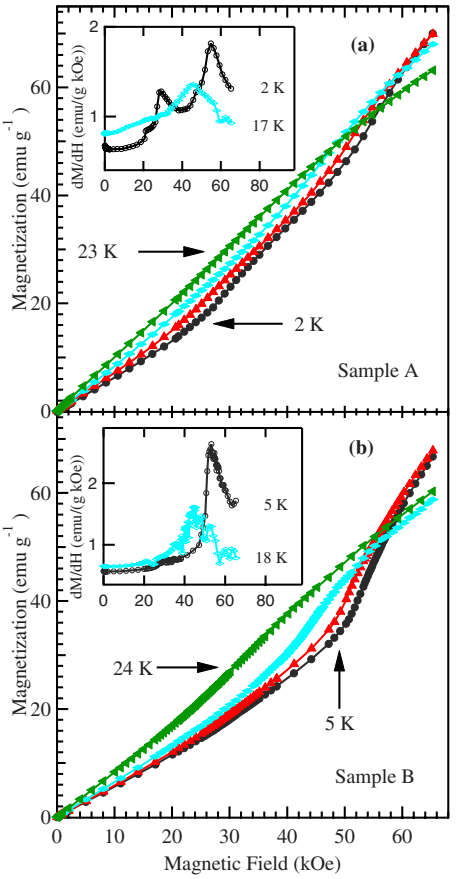

FIG. 7. (Color online) M vs H variations are shown for T =2(5), 11 (14), 17 (18), and 23 (25) K for sample A (sample B). The inset shows dM/dH for two select temperatures.

puted $d(\chi T)/dT$ are shown in Fig. 6(a). Here T_1 is a broad minimum near 35 K, whereas the transition at $T_2 \simeq 25.5$ K is a λ-type anomaly characteristic of specific heat anomaly at a phase transition.[21,22] The relationship of the shift of T_1 to higher temperatures in sample B with its larger size needs further investigations.

B. Magnetic field dependence

For sample A, variation of the magnetization (M) with applied magnetic field (H) up to ±65 kOe was investigated at 18 selected temperatures between 2 K and 28 K both for the ZFC and the FC cases, the latter by cooling the sample in 25 kOe. For sample A (sample B), the data of M vs H for the ZFC case at T=2(5), 11 (14), 17 (18), and 23 (25) K as the representative temperatures are shown in Fig. 7. The inset of Fig. 7 shows computed $\frac{\partial M}{\partial H}$ vs H for two select temperatures. The presence of two peaks in $\frac{\partial M}{\partial H}$ at $H_{C1} \simeq 28$ kOe and $H_{C2} \simeq 55$ kOe is quite evident for sample A. Similar data and analysis for sample B show only a single peak at $H_{C2} \simeq 53$ kOe. In both cases, the position of the peaks shifts to lower H at higher T. In the earlier studies of bulklike β-Ni(OH)$_2$ in Ref. 10, the observed transition at 55 kOe was related to metamagnetism, i.e., magnetic field-induced transition from AFM order to FM order for $H > H_{C2} \simeq 55$ kOe. Later we further elaborate on this metamagnetism and related

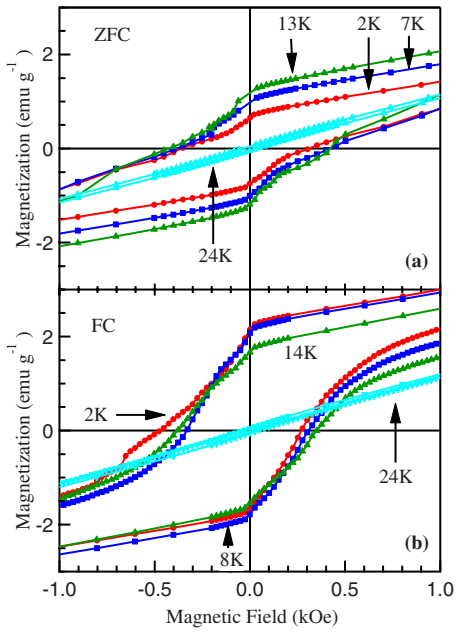

FIG. 8. (Color online) Shown are the M-H loops of sample A for the (a) zero-field-cooled case at T=2, 7, 13, and 24 K and (b) field-cooled (H=25 kOe) case at T=2, 8, 14, and 24 K.

properties by including the temperature dependence of H_{C1} and H_{C2} and interpretation of H_{C1} which have not been reported before.

In Ref. 11, the observation of the hysteresis in M vs H at 10 K for the 8 nm β-Ni(OH)$_2$ along with positive θ was used as an evidence for FM order. We measured the temperature dependence of the coercivity (H_c) and exchange-bias (loop shift, H_{eb}) for sample A for the ZFC and FC (25 kOe) cases. The low-field regions of the M-H loop at the select temperatures of 2, 7, 13, and 24 K for the ZFC case are shown in Fig. 8(a). Similar data for the select temperatures of 2, 8, 14, and 24 K for the FC case (cooled in H=25 kOe) are shown in Fig. 8(b). Temperature dependence of H_c(ZFC), H_c(FC), H_{eb}(ZFC), and H_{eb}(FC) determined from this data is shown in Fig. 9(b). As T is lowered below T_N, H_c increases rapidly approaching maximum $H_{c,max}$=470 Oe at 20 K. Below 20 K, the temperature variation in both H_c(ZFC) and H_c(FC) is rather monotonic with H_c(FC) generally lower than H_c(ZFC). The magnitudes of H_{eb}(ZFC) and H_{eb}(FC) are quite small (±10 Oe), being positive for the ZFC and negative for the FC cases. Since the accuracy of measuring and setting the field in the SQUID is about ±10 Oe, we do not attach a great deal of significance to this small observed H_{eb}. The remanence (M_r) measured in the limit $\vec{H} \to 0$ from the hysteresis curves of Fig. 8 are plotted against temperature [Fig. 9(a)] for both the ZFC and FC cases for sample A. M_r goes to zero on approach to T_N and M_r(FC) > M_r(ZFC) essentially for all temperatures up to T_N. The maximum magnitude of M_r for sample A is about 2% of saturation magnetization measured at 150 kOe. For the bulklike sample B, the coercivity H_c at 5 K was only about 40 Oe with remanence $M_r \simeq 0.04$ emu/g. Since these magnitudes are rather negligible compare to $H_c \simeq 470$ Oe and $M_r \simeq 2$ emu/g for sample A, it is safe to assume that in a bulklike sample, both

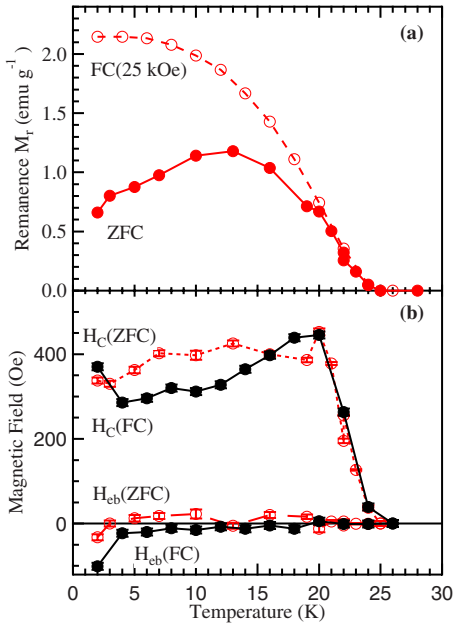

FIG. 9. (Color online) (a) For sample A, temperature variations in the remanence for the ZFC and FC (25 kOe) case. The lines joining the points are for visual clarity. (b) For sample A, temperature variations in the coercivity (H_c) and exchange bias (H_{eb}) for the ZFC and FC (25 kOe) case. The lines joining the points are for visual aid.

H_c and M_r are zero and that bulk β-Ni(OH)$_2$ is an antiferromagnet at $H=0$.

In the M vs H variation in Fig. 7, M is not saturated even at 65 kOe. Consequently, the high magnetic field facilities of the NHMFL (Tallahassee, FL) were employed to measure the magnetic susceptibility (χ) of sample A up to 180 kOe. In these measurements, χ was measured using an ac method while sweeping the field from 0 to 180 kOe in about 30 min. This data of χ vs H at $T=2$ K for sample A is plotted in Fig. 10(a). The two observed peaks in χ at $H_{C1} \simeq 33$ kOe and $H_{C2} \simeq 54$ kOe are identical to the data shown in Fig. 7(a) for sample A taken with the SQUID magnetometer. By integrating the χ vs H data of Fig. 10(a), magnetization was obtained and the plot of M vs H is shown in Fig. 10(b), where we have also included the data taken with the SQUID up to 65 kOe. Note the computed values of M vs H were normalized with the SQUID data at the single magnetic field $H=65$ kOe. Above 150 kOe, M is practically saturated with the saturation value $M_s=118$ emu/g. Because the sample is polycrystalline, M is not saturated at $H=H_{C2}$. An interpretation of this as well as the peaks at H_{C1} and H_{C2} is given later in Sec. IV.

C. Temperature dependence of the critical fields

The temperature dependence of H_{C1} and H_{C2} determined using the data taken with the SQUID as well as the data taken at the NHMFL for sample A is plotted in Fig. 11(b). For H_{C1}, no data above 15 K is shown since the peak became too faint to detect. For H_{C2}, it is safe to infer by extrapolation that its magnitude goes to zero as $T \rightarrow T_N$. Similar data for

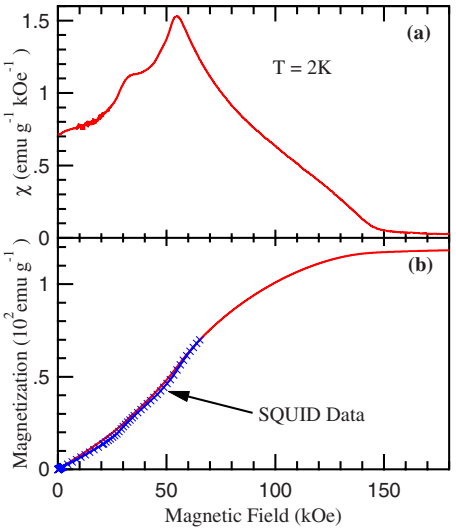

FIG. 10. (Color online) (a) Magnetic susceptibility of sample A at $T=2$ K measured vs H at the NHMFL is shown as the solid line. (b) The magnetization derived from the magnetic susceptibility of the NHMFL data and normalized to the SQUID data at $H=65$ kOe.

H_{C2} in sample B is shown in Fig. 11(a). Of course the peak related to H_{C1} is not observed in sample B. The solid curve is the calculated Brillouin function variation for spin $S=1$ of Ni^{2+}.[23] Note that in Fig. 11(b), both H_{C1} and H_{C2} are normalized to $H_{C2}(0)=54.5(1.0)$ kOe, whereas in Fig. 11(a) H_{C2} is normalized to $H_{C2}(0)=53.5(1.0)$ kOe.

IV. DISCUSSION AND INTERPRETATION

For a ferromagnet in the limit $T \rightarrow 0$ K, $M_S=Ng\mu_B\langle S\rangle$. For β-Ni(OH)$_2\cdot 0.15H_2$O, using $g=2.2$ and $S=0.92$ yields the calculated $M_S=118.5$ emu/g, in excellent agreement with the experimental $M_S=118$ emu/g determined above in Fig. 10 for $H>145$ kOe when the system is in the FM state. We next address the origin for H_{C2} and the equality $H_{C1} \simeq H_{C2}/2$ by deriving expressions for H_{C2} and H_{C1} using a molecular field approach. As noted earlier, the Ni^{2+} spins in β-Ni(OH)$_2$ in the AFM state are parallel along the c axis within each c plane with the alternate c planes aligned antiferromagnetically. We are using a two-sublattice model, the standard procedures for the molecular-field model,[23] and the Hamiltonian

$$\mathcal{H} = -2\sum_{i,j} J_{ij}\vec{S}_i \cdot \vec{S}_j - g\mu_B\vec{H} \cdot \sum_i \vec{S}_i \qquad (2)$$

Assuming Ising-type ordering, $\vec{H}\|$ to the c axis, and the three exchange interactions J_1, J_2, and J_3 [Fig. 1(a)], the following equations for θ and T_N are obtained

$$3k\theta = 2S(S+1)[J_1Z_1 + (J_2Z_2 + J_3Z_3)], \qquad (3)$$

$$3kT_N = 2S(S+1)[J_1Z_1 - (J_2Z_2 + J_3Z_3)], \qquad (4)$$

where k is the Boltzmann constant and $Z_1=6$, $Z_2=2$, and $Z_3=12$ are the appropriate number of neighbors involved in

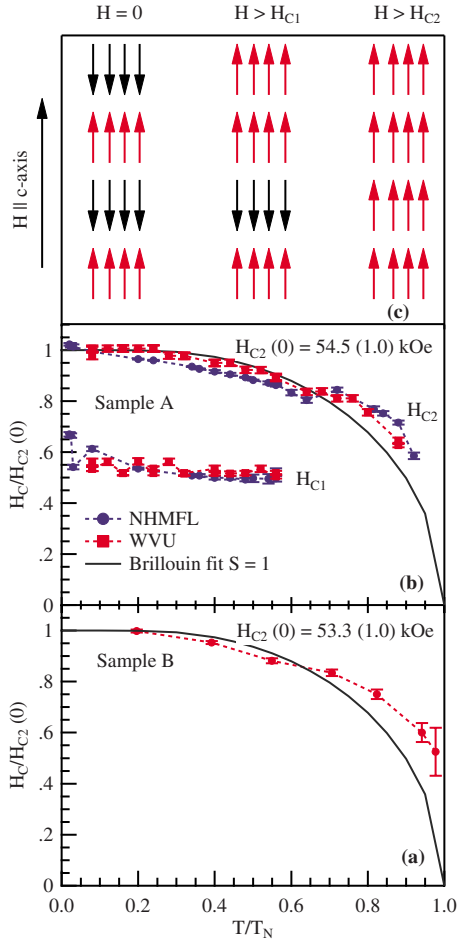

FIG. 11. (Color online) Temperature variation in the critical fields H_{C1} and H_{C2} using $T_N=25$ K for sample A and $T_N=25.5$ K for sample B. For sample B, H_{C1} is not observed and the solid lines in both (a) and (b) represent the Brillouin function variation for $S=1$. (c) Schematic representations for the magnetic field-induced spin ordering at the three cases shown.

the exchange constants J_1, J_2, and J_3, respectively, for the hexagonal lattice shown in Fig. 1. To obtain an equation for H_{C2} for the transition from the AFM state in $H=0$ to the FM state for $H \geq H_{C2}$ applied along the c axis, we compare the energies of the two states using the Hamiltonian in Eq. (2)

$$E_{\uparrow\downarrow} = -2NS^2[J_1Z_1 - (J_2Z_2 + J_3Z_3)], \tag{5}$$

$$E_{\uparrow\uparrow} = -2NS^2[J_1Z_1 + (J_2Z_2 + J_3Z_3)] - Ng\mu_B SH. \tag{6}$$

For $E_{\uparrow\downarrow}=E_{\uparrow\uparrow}$ at $H=H_{C2}$ yields

$$H_{C2} = -4S(J_2Z_2 + J_3Z_3)/(g\mu_B) \tag{7}$$

The signs and magnitudes of J_1, J_2, J_3, and H_{C2} are now calculated using the above derived equations for θ, T_N, and H_{C2}. For sample A, $\theta=20.5$ K and we take $T_N=25$ K (the temperature at which 2D ordering sets in). Use of these magnitudes of θ and T_N with $g=2.2$ and $S=0.92$ in Eqs. (3) leads to $J_1/k=3.25$ K, and $(J_2Z_2+J_3Z_3)/k=-1.91$ K. Following the arguments in Ref. 6, $J_2=3J_3$ is assumed leading to $J_2/k=-0.32$ K and $J_3/k=-0.11$ K. The signs and magnitudes of the exchange constants J_1, J_2, and J_3 determined above implies that the dominant intraplanar exchange (J_1) is ferromagnetic, and it is an order of magnitude larger than the interplanar antiferromagnetic exchange constants (J_2 and J_3). Similar analysis for sample B with $\theta=19.8$ K and $T_N=25.5$ K [Figs. 4(c) and 6(a)] yields $\mu=3.3$ μ_B/Ni^{2+} ion and $J_1/k=2.67$ K and $J_2/k=3J_3/k=-0.315$. In the earlier studies of bulklike β-Ni(OH)$_2$ (Ref. 6) $J_1/k=2.70$ K, $J_2/k=-0.28$ K, and $J_3/k=-0.09$ K were reported. So the signs and magnitudes of the exchange constants determined here for our sample B and those determined in Ref. 6 for bulklike β-Ni(OH)$_2$ are nearly the same.

Next, Eq. (7) and the exchange constants determined above are used to determine the magnitude of H_{C2} for the two cases discussed above. For $S=0.92$ as in sample A, $H_{C2}=47.6$ kOe is calculated using Eq. (7), whereas for the $S=0.97$ case, $H_{C2}=51.8$ kOe is determined. These magnitudes are in good agreement with the experimental value of $H_{C2} \simeq 55$ kOe considering that the calculations of H_{C2} were determined using parameters determined from the data for $T > T_N$, whereas the experimental value of 55 kOe is measured at 2K. According to Eq. (7), the temperature dependence of H_{C2} should be governed by the temperature dependence of $\langle \vec{S} \rangle$, which reflects the order parameter. The solid line in Fig. 11 is the Brillouin function variation for $S=1$ (Ref. 24) showing agreement with the temperature variation of the data for H_{C2} for our samples except for the region close to T_N where experimental values of H_{C2} are consistently higher for both samples. Some comments on their disagreement are made later. Furthermore, this analysis shows that for the metamagnetic transition to FM order, the required magnetic field needs to overcome the interplanar AFM coupling only [Eq. (7)]. Since our measurements have been carried out on polycrystalline samples, the observed transition at H_{C2} is somewhat weakened because only a fraction of the crystallites are oriented with $\vec{H} \| c$ axis.

For Ni^{2+} spins on the surface layer of a (00ℓ)-oriented nanoplate of β-Ni(OH)$_2$, the number of next-nearest neighbors ($Z_2=1$ and $Z_3=6$) are just half the number for spins on a layer deep inside the nanoplate. Although $Z_1=6$ is unchanged for the surface layer, Eq. (7) does not depend on Z_1. Therefore, the field required to switch the moments of a surface layer is just half of H_{C2}. This field is associated with H_{C1} observed here following the suggestion of Miyamoto.[25] Although Miyamoto did not carry out any calculations for H_{C1} or H_{C2}, the gradual weakening of the peak associated with H_{C1} was reported as the particle size increased.[25] Thus $H_{C1}=H_{C2}/2$ represents the switching of the moments on the surface layer from the antiparallel to a direction parallel to the applied magnetic field [Fig. 11(c)]. The peak associated with H_{C1} weakens with increase in particle size because the fraction of spins on the surface to the total number of spins in the sample decreases with increase in size. Thus the absence of a peak related to H_{C1} in bulklike sample B can be understood.

The magnetic field $H_S \simeq 150$ kOe required to saturate the magnetization (Fig. 10) is much larger than the field $H_{C2} \simeq 55$ kOe needed for metamagnetic transition. This apparent anomaly results from the fact that in a powder sample on

average, $\chi_p=(\chi_\parallel+2\chi_\perp)/3$ is measured where $\chi_\parallel$ ($\chi_\perp$) is the susceptibility for $\vec{H}\parallel(\perp)$ to the c axis. Whereas H_{C2} corresponds to metamagetism for $\vec{H}\parallel c$ axis, H_S is interpreted to be the field required to saturate $\chi_\perp$ when $M_\perp=M_\parallel$. Using $\chi_\perp=7.71\times10^{-4}$ emu/(g Oe) reported by Takada *et al.*,[10] $H_S=M_S/\chi_\perp=153$ kOe is calculated for $M_S=118$ emu/g. This is in good agreement with $H_S\simeq150$ kOe evident in the data of Fig. 10.

The remanence (M_r) and its temperature dependence is likely associated with the particle size effect also since studies by Miyamoto[25] on four different particle sizes of β-Ni(OH)$_2$ showed M_r to increase with decrease in particle size. An explanation for this effect is as follows. For even number of (00ℓ) layers in nanoplates, the moments are compensated for $H=0$ and $T\rightarrow0$, leading to AFM order and zero M_r. However, for odd number of layers, there are uncompensated moments yielding M_r. Based on the statistical orientation of a polycrystalline sample, on average only 1/3 of the particles will be oriented with $\vec{H}\parallel c$ axis, and the number of crystallites with odd number of layers on average equal about half of the total number. The number of uncompensated surface layers depends on the total $(2m+1)$ odd number of layers. These factors lead to $M_r=\frac{M_s}{6(2m+1)}$ with $m=4$ for our sample with plate thickness $d=4.3$ nm using $c=0.467$ nm. This yields $M_r\simeq2.2$ emu/g, in close agreement with the measured value for the FC case at 2 K [Fig. 9(a)]. The temperature dependence of M_r for the FC case closely follows the Brillouin function variation for $S=1$ as expected. The peak in M_r(ZFC) near 15 K [Fig. 9(a)] is not yet understood.

The sharp rise of χ(FC) in Fig. 4(a) for $T<T_p$ is observed only in sample A but not in bulklike sample B. A similar rise for χ(FC) in the 8 nm sample of Ref. 11 was also reported. Therefore, it is inferred that this effect is present only in nanoparticles. It is very likely that this effect is due to the uncompensated spins of the odd number of layers and the fact that H_{C1} is also likely zero at T_N. Thus nanoplates of β-Ni(OH)$_2$ display the unique characteristics of both FM and AFM orders depending on whether the sample is cooled to $T<T_N$ in a magnetic field or in zero field.

In Fig. 11 it is evident that in the temperature variation in H_{C2} on approach to T_N, the observed magnitudes of H_{C2} are higher than the predicted Brillouin function variation for $S=1$ based on the molecular field approximation. Theoretically, Fox and Guttmann[26] have examined the low-temperature critical behavior of the Ising model for $S=1$ and $S=3/2$ using the low-temperature series expansions. Their results for the triangular and bcc lattices on the variation of $\langle S\rangle$ against T/T_C show that for a given T/T_C on approach to T_C, the calculated magnitude of $\langle S\rangle$ is larger than that predicted by the molecular field theory. This is qualitatively similar to our observation in Fig. 11 for both samples A and B. However a quantitative test is not possible because the dependence of the calculations on the lattice type and size dependence is not addressed in Ref. 26.

Our final comment is on the observed magnetic field variation of T_1 and T_2 in Fig. 6. Whereas T_1 associated with 2D FM ordering is essentially independent of H, T_2 associated with 3D AFM ordering varies nearly as $H^{1/2}$. Bienenstock[27] has calculated the variation in T_N in Ising antiferromagnets with H using high-temperature series expansion, yielding $T_C(H)/T_C(0)=[1-(H/H_K)^2]^\xi$ with $\xi=0.87$, 0.35, and 0.36 for square, SC, and bcc lattices. The importance of these predictions is that for 3D ordering, change in $T_C(H)$ with H is much weaker than the H^2 dependence, as observed here for T_2 in β-Ni(OH)$_2$. However, without an accurate knowledge of H_K, a more quantitative comparison is not possible.

V. CONCLUDING REMARKS

Detailed measurements of the magnetic properties of the layered antiferromagnet β-Ni(OH)$_2$ have been compared for two samples, viz., sample A with nanoplate morphology and bulklike sample B along with theoretical interpretation of the results using a molecular field approach. These investigations have clearly established this material to be a metamagnet with a critical field $H_{C2}\simeq55$ kOe associated with the transition from antiferromagnetism for $H<H_{C2}$ to ferromagnetism for $H>H_{C2}$ for $\vec{H}\parallel c$ axis. Moreover, the observed $H_{C1}\simeq28$ kOe in sample A only is associated with the magnetic field-induced flipping of the Ni^{2+} moments on the surface layers whose relative fraction increases with decrease in the thickness of the nanoplates. Therefore, the observation of H_{C1} is a size-dependent effect. Similarly the observed remanence and coercivity in sample A for $T<T_N$ is also a nanosize effect related to uncompensated surface layers. In contrast, in bulklike sample B H_{C1} is not observed and remanence and coercivity for $T<T_N$ are negligible. Because the in-plane exchange coupling is ferromagnetic and it is also an order of magnitude larger than the AFM interplane coupling, it leads to the observed two-step magnetic ordering on lowering the temperature: FM ordering of the Ni^{2+} moments in the (00ℓ) layers at a higher temperature T_1 followed by long-range AFM ordering at a lower temperature T_2. Using a molecular field approach, expressions for H_{C1} and H_{C2} are derived in terms of the exchange constants and the theoretical estimates of H_{C1} and H_{C2} are in good agreement with the observed values. Similarly, the observed magnitude of remanence is satisfactorily explained. Finally, the observed temperature dependence of H_{C2} in samples A and B are compared with the Brillouin function variation for $S=1$; the observed disagreements on approach to T_N are discussed in terms of the breakdown of the molecular field approximation near T_N.

ACKNOWLEDGMENTS

Research at West Virginia University was supported in part by the U.S. Department of Energy (Contract No. DE-FC26-05NT42456). A portion of this work was performed at the National High Magnetic Field Laboratory, which is supported by NSF Cooperative under Agreement No. DMR-0654118, by the State of Florida, and by the DOE.

*Author to whom correspondence should be addressed; mseehra@wvu.edu

[1] For earlier studies on lower *D* magnetic materials, see the review by L. J. de Jongh and A. R. Miedema, Adv. Phys. **23**, 1 (1974); also see the more recent monograph *Magnetic Properties of Layered Transition Metal Compounds*, edited by L. J. de Jongh (Kluwer Academic, Boston, 1990).

[2] D. J. Sellmyer, M. Zheng, and R. Skomski, J. Phys.: Condens. Matter **13**, R433 (2001).

[3] See, e.g., *Nanomaterials and Nanochemistry*, edited by C. Brechignuc, P. Houdy, and M. Lehmani (Springer, New York, 2007).

[4] See the review by A. Lu, E. L. Salabas, and F. Schuth, Angew. Chem., Int. Ed. **46**, 1222 (2007).

[5] Potential applications of magnetic nanoparticles are discussed in a number of reviews/publications and references therein; e.g., see Q. A. Pankhurst, N. K. T. Thanh, S. K. Jones, and J. Dobson, J. Phys. D: Appl. Phys. **42**, 224001 (2009); P. I. Nikitin, P. M. Vetoshko, and T. I. Ksenevich, J. Magn. Magn. Mater. **311**, 445 (2007); E. R. Leite, N. L. V. Carrerio, E. Longo, A. Valentini, and L. F. D. Probst, J. Nanosci. Nanotechnol. **2**, 89 (2002); D. L. Leslie-Pelecky, and R. D. Rieke, Chem. Mater. **8**, 1770 (1996).

[6] T. Enoki and I. Tsujikawa, J. Phys. Soc. Jpn. **39**, 317 (1975); **45**, 1515 (1978).

[7] T. N. Ramesh, Mater. Chem. Phys. **114**, 618 (2009); T. N. Ramesh and P. V. Kamath, Mater. Res. Bull. **43**, 3227 (2008); **43**, 2827 (2008).

[8] P. Oliva, J. Leonardi, J. F. Laurent, C. Delmas, J. J. Braconnier, F. Figlarz, F. Fievt, and A. de Guibert, J. Power Sources **8**, 229 (1982).

[9] A. Szytula, A. Murasik, and M. Balanda, Phys. Status Solidi B **43**, 125 (1971).

[10] T. Takada, Y. Bando, M. Kiyama, H. Miyamoto, and T. Sato, J. Phys. Soc. Jpn. **21**, 2726 (1966); **21**, 2745 (1966); H. Miyamoto, Bull. Inst. Chem. Res., Kyoto Univ. **44**, 420 (1966).

[11] S. D. Tiwari and K. P. Rajeev, Phys. Rev. B **77**, 224430 (2008).

[12] J. D. Rall, M. S. Seehra, N. Shah, and G. P. Huffman, J. Appl. Phys. **107**, 09B511 (2010).

[13] H. P. Klug and L. E. Alexander, *X-Ray Diffraction Procedures*, 2nd ed. (Wiley, New York, 1974); M. S. Seehra and A. S. Pavlovic, Carbon **31**, 557 (1993).

[14] Z.-H. Liang, Y.-J. Zhu, and X.-L. Hu, J. Phys. Chem. B **108**, 3488 (2004).

[15] L.-X. Yang, Y.-J. Zhu, H. Tong, Z.-H. Liang, L. Li, and L. Zhang, J. Solid State Chem. **180**, 2095 (2007).

[16] M. S. Seehra, P. Roy, A. Raman, and A. Manivannan, Solid State Commun. **130**, 597 (2004).

[17] A. Punnoose, H. Magnone, M. S. Seehra, and J. Bonevich, Phys. Rev. B **64**, 174420 (2001); T. Ambrose and C. L. Chien, Phys. Rev. Lett. **76**, 1743 (1996); Y. J. Tang, D. J. Smith, B. L. Zink, F. Hellman, and A. E. Berkowitz, Phys. Rev. B **67**, 054408 (2003); X. G. Zheng, C. N. Xu, K. Nishikubo, K. Nishiyama, W. Higemoto, W. J. Moon, E. Tanaka, and E. S. Otabe, *ibid.* **72**, 014464 (2005).

[18] G. Guisbiers and L. Buchaillot, Phys. Lett. A **374**, 305 (2009); X. Y. Lang, W. T. Zheng, and Q. Jiang, Phys. Rev. B **73**, 224444 (2006).

[19] V. Singh, M. S. Seehra and J. Bonevich, J. Appl. Phys. **105**, 07B518 (2009); H Shim, A. Manivannan, M. S. Seehra, K. M. Reddy and A. Punnoose, *ibid.* **99**, 08Q503 (2006).

[20] G. Srinivasan and M. S. Seehra, Phys. Rev. B **29**, 6295 (1984), and references therein.

[21] M. E. Fisher, Philos. Mag. **7**, 1731 (1962).

[22] E. E. Bragg and M. S. Seehra, Phys. Rev. B **7**, 4197 (1973); W. P. Wolf and A. F. G. Wyatt, Phys. Rev. Lett. **13**, 368 (1964); J. Skalyo, Jr., A. F. Cohen, S. A. Friedberg, and R. B. Griffiths, Phys. Rev. **164**, 705 (1967).

[23] *The Physical Principles of Magnetism*, edited by A. H. Morrish (IEEE Press, New York, 2001), p. 447.

[24] M. I. Darby, Br. J. Appl. Phys. **18**, 1415 (1967).

[25] H. Miyamoto, Mater. Res. Bull. **11**, 599 (1976).

[26] P. F. Fox and A. J. Guttmann, J. Phys. C **6**, 913 (1973).

[27] A. Bienenstock, J. Appl. Phys. **37**, 1459 (1966).